

International Journal of Current Bio-Medical Engineering (IJCBE) Volume 3, Issue 1, January – February (2025)

RESEARCH ARTICLE

ABDOMINAL AORTIC ANEURYSM DETECTION USING EFFECTIVE MODIFIED DEEP V3+ NET

J. Sworna Jo Lijha ^{1,*}, N. Muthukumaran ²

¹ Assistant Professor, Department of Electronics and Communication Engineering, Sree Sakthi Engineering College, Coimbatore, Tamilnadu, India

² Professor, Department of Electronics and Communication Engineering, Sri Eshwar College of Engineering, Coimbatore, Tamil Nadu, India

*Corresponding e-mail: jswornajolijha@gmail.com

Abstract - The prediction of Abdominal Aortic Aneurysm (AAA) develpoment is crucial to early treatment and surgical intervention. It is critically important to capture key vascular growth factors like blood flow and intraluminal thrombus (ILT) accumulation in order to understand how vascular adaptation occurs. In this paper a novel has been proposed for detecting the AAA. Initially the input CT images are pre-processed using AUG filter to enhance the quality of the images. Then the enhanced images are fed into Modified Deep V3+ for segmenting the required features from the image. The segmented images are inputted into feature extraction process for extracting the required features using Effective Net. Finally, the normal and abnormal classes of the aortic aneurysm detection is classified using DBN classifier. The proposed archives an accuracy rate of 99.34% in the normal classes and 99.28% in the abnormal classes. The accuracy rating of 99.31% achieved by the suggested is higher than that of the current techniques. In this, the proposed achieves an overall accuracy rate of 0.77%, 0.31% and 1.17% over the existing methods such as CTA, PRAEVAorta and ATAAs respectively.

Keywords – Abdominal Aortic Aneurysm (AAA), AUG filter, Modified Deep V3+, DBN, computed tomography (CT).

1. INTRODUCTION

ISSN: XXXX-XXXX

An abdominal aortic aneurysm can result in life-threatening bleeding, and rupture is associated with a mortality rate exceeding 50% [1]. Abdominal computed tomography (CT) scans performed for a number of reasons in clinical practice may show small AAA, a low prevalence condition, as a co-finding [2]. The focus on other clinical issues and the time-consuming nature of a comprehensive AAA examination may result in underreporting and a delayed diagnosis [3]. Patients might thus be released without an early AAA being discovered. Given the shown benefits of surveillance programs, this could result in a delay in treatment [4]. Larger AAAs can ultimately be treated surgically or interventional to prevent spontaneous rupture [5]. In modern clinical practice, AAAs are typically found as unintentional results of magnetic resonance imaging,

abdominal computed tomography, or ultrasonography that is done for another reason [6]. Unfortunately, the equipment needed for these medical imaging tests is specialized and not applicable to everyday life [7]. The key structural proteins in the aorta wall, collagen and elastin, are altered in AAA, leading to irreversible swelling and a loss of structural integrity [8]. The most popular imaging screening method for AAA is ultrasound, which has been shown to be both more affordable and more successful than traditional computed tomography (CT) scans. However, highly skilled sonographers typically perform ultrasounds, and boardcertified doctors evaluate the results [9]. This difficulty is made worse by the limited availability of advanced ultrasonography equipment [10]. These two problems reduce the cost-effectiveness of general screening for AAA, which also contribute to the longest wait times for ultrasound exams when compared to other imaging modalities. The research focused on severe infrarenal AAAs, as further validation is required to accurately characterize patients with complex aneurysms using deep learning (DL) networks such as Autoencoder [11], YOLO [12], and others. To overcome this, a novel has been proposed for detecting the abdominal aortic aneurysm.

- Initially the input CT images are pre-processed using AUG filter to enhance the quality of the images.
- Then the enhanced images are fed into Modified Deep V3+ for segmenting the required features from the image.
- The segmented images are inputted into feature extraction process for extracting the required features using Effective Net.
- Finally the normal and abnormal classes of the aortic aneurysm detection is classified using DBN classifier.

©KITS PRESS Publications

The format for the remainder of the study report was as follows. Section 2 provides an overview and a full summary of the relevant works. A thorough description of the proposed system for aortic aneurysm detection is provided in Section 3. The experimental fallouts and discussion are in Section 4. Section 5 concludes with some thoughts for future development.

2. LITERATURE SURVEY

In 2020 Joo, B et al [13] suggested a DL method to assess the diagnostic performance of time-of-flight MR angiography in order to automatically locate and identify brain aneurysms. A training set of 468 tests and an internal test set of 120 tests were randomly selected from the test data. An external data set was utilized to validate the exceptional diagnostic capabilities of a deep learning algorithm that identified brain aneurysms. The internal test set had 87.1%, 92.8%, and 92.0% sensitivity, specificity, and positive predictive value, while the external test sets had 85.7%, 91.5%, and 98.0%, respectively.

In 2022 Brutti, F. et al [14] suggests a completely automated method to analyze AAA shape after segmenting the contrast-enhanced Computed Tomography Angiography (CTA) pictures of the intraluminal thrombus associated with AAA. The recommended multi-view integration method improves the thrombus segmentation as compared to the single-view prediction. The deep learning algorithms that have been built are capable of efficiently separating the thrombus from AAA patients.

In 2021 Caradu, C. et al [15] developed PRAEVAorta, an automated program that allows in order to quickly and accurately determine the AAA features intrarenal, such as the presence of thrombus, and the aortic lumen. The investigations demonstrated excellent correlations between the diameters, volumes, and surfaces recorded using the fully automatic and manually modified segmentation methods. The fully automated method's segmentation time ranged from 27 seconds to 4 minutes per patient (P <.0001), while the manually corrected techniques ranged from 5 to 80 minutes. The results shown that in 100 CTAs with different infrarenal AAA anatomies, these fully autonomous identification algorithms were accurate and dependable.

In 2021 Comelli, A. et al [16] created a deep learning technique utilizing UNet, ENet, and ERFNet to automatically partition ATAAs. The segmentation performance in terms of accuracy and time inference was

compared using a variety of criteria. A dice scores greater than 88% was recorded by all deep learning models, indicating a high degree of agreement between the manual and predicted ATAA segmentation. Deep learning for autonomous vascular segmentation in clinical settings can enhance more than just ATAA diagnosis.

In 2021 Tahoces, P.G., et al [17] proposed an automated technique that does not require prior segmentation to identify the aortic root in CTA imaging. The suggested approach makes an effort to resemble the standard practice followed by an expert. CNN-based models are used by the created algorithm to accomplish this objective. Datasets containing few examples are used to train the models. The outcomes show how transfer learning makes it possible to achieve reasonable outcomes in this kind of process, and they seem to be optimal.

In Kim, S. et al [18] developed a deep learning framework for predicting AAA growth that was learned using multi-physical features and a deep convolution neural network. It can assist medical professionals in managing AAA while providing better patient care. The results illustrate the impact of utilizing multi-physical features and indicate how the architecture that was presented outperformed earlier state-of-the-art techniques in predicting AAA growth. The method will clarify deep learning models based on physics for use in biomedical applications.

In 2022 Hu, T. at al [19] suggested a deep learning technique that takes into account the aorta to create arterial contrasted CT volume from non-contrast CT volume. The greatest axial radius of the aorta was estimated in order to detect aberrant CT pictures that contained aneurysms. By focusing on aortic areas, the auxiliary tasks enable the proposed model to synthesis findings with more distinct boundaries. Furthermore, the synthetic artery contrasted CT scan has the ability to detect slices with abdominal aortic aneurysms and could be a viable alternative for patients who are allergic to contrast agents. The Architecture of Proposed Method is shown in Figure 1.

3. PROPOSED METHOD

In this section, a novel modified deep v3+ net for effective AAA detection using CT images. The Architecture of Proposed Method is shown in Figure 1.

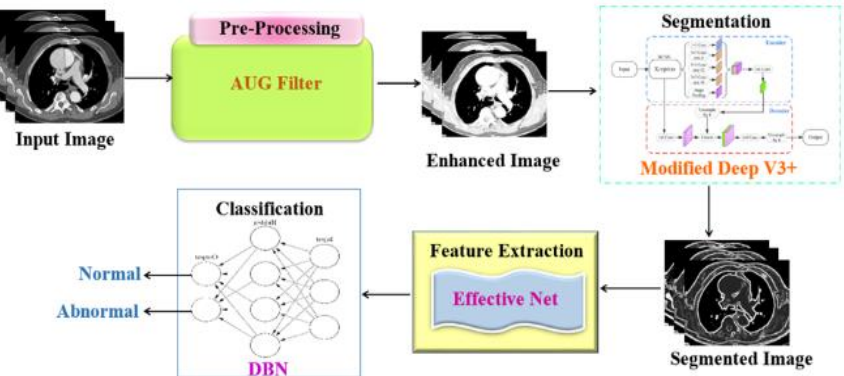


Figure 1. Architecture of Proposed Method

3.1. Data Pre-Processing

The AUG filtering technique is used to pre-process the input data in order to improve the images. The most common kind of computational filter used to enhance images in digital imaging is the AUG filter. Adaptive filters modify their filtering coefficients according to the distinct appearance factors, in contrast to classic effects that depend on a predetermined set of parameters. Adaptive filtering preserves patterns and minimizes disturbances by modifying the filtration kernel according to the distinct features of a picture. equation (1) states that the logical unsharp masking process uses the input picture d(w, u) to create the enhanced image

$$a(w,u) = d(w,u) + \beta x(w,u) \tag{1}$$

Where β is the scaling coefficient that controls the amount of enhanced contrast at the output, and x(w, u) is the corrected data computed as the outcome filter. A common strategy used in image enhancement methods is to generate x(w, u) as the improve filters, equation (2).

$$x(w,u) = 4a(w,u) - a(w-1,u) - a(w+1,u) - a(w,u-1) - a(w,u+1)$$
(2)

The AUG Filter is an image enhancement technique that minimizes distortion and highlights features functions, equation (3).

$$I_n = f_n(I_n, g) \tag{3}$$

The following equation represents the guided image enhanced filter: (4). Let I_n denote the filtered image's result, and let $f_n(.)$ stand for the improved CT image.

3.2. Modified Deep V3+ for segmentation

One prominent technique for semantic segmentation of aortic aneurysm CT images is Deeplabv3+, which has shown promising results. DeepLabV3+ uses two deep neural network encoders and decoders as well as the spatial pyramids pooling unit. To increase the speed and efficiency of the connection, depth-wise separable convolution is applied to the decoder module and spatial pyramid pooling while continually monitoring the backbone for the feature extraction system. The encoding system consists of a backbone network and an ASPP module, which are integrated into the network's decoder section. An encoderdecoder form is added to the Deeplaby 3+, a semantic segmentation network, to facilitate the fusion of multi-scale data. The convolution kernel (v), the output $\mathcal{P}[q]$, the expansion factor a_h , the input I, and the proper sequence number n between the input and the output is expressed using a two-dimensional signal as an example. The null convolution is equivalent to injecting $a_h - 1$ zeros into the input I in each channel dimension and convolving it between the convolution kernels created by two subsequent convolution kernels, as can be seen in the following equation

$$\mathcal{P}[q] = \sum_{\mathfrak{n}} \mathfrak{w} \mathbb{I} \left[\mathfrak{h} + a_{\mathfrak{h}} \times \mathfrak{w} \right] k[\mathfrak{n}] \tag{4}$$

Ghost Net is appropriate for applications with limited resources because of its lightweight and computationally efficient design. It maintains strong segmentation performance while lowering overall processing needs when utilized as the backbone of DeepLabv3+. A single-channel grayscale image or a three-channel RGB image, depending on the input data, is usually used as the input for the input layer. The convolutional blocks employed by Ghost Net consist of a series of point wise convolutions that accompany standard depth-wise convolutions. These segments record different feature data levels of the input image. The output is combined by the pointwise convolution, but the depth wise convolution processes each input channel independently. A few actions are necessary in order to identify relevant features for segmentation jobs. On the CNN network, a ghost unit has been implemented to decrease network traffic, enhance feature benefits, and extract bottom-level parameters on several layers.

According to the information, the number of variables for the convolutional layers is $\mathcal{P} \in \mathcal{R}^{\mathcal{X}_{\mathcal{V}} * \mathcal{X}_{\mathcal{V}} * \mathcal{T}_{\mathcal{V}-1} * \mathcal{B}_{\mathcal{V}-1}}$, where $\mathcal{X}_{\mathcal{V}}$, shows the filter's dimensions as well as breadth $\mathcal{B}_{\mathcal{V}-1}$ specifies data from the source path and $\mathcal{B}_{\mathcal{V}}$ represent the number of filters. Apply the linear model obtained from equation (5) to find the \mathfrak{w}^{th} layering function for this design. The segmented vector connection for the input data is given by combining the equivalent $\mathcal{R}_{n-1} \in \mathcal{P}^{\mathcal{D}_{u-1} * \mathcal{Z}_{u-1} * \mathcal{C}_{u-1}}$. This leads to the creation of a random output map of segmented features $\mathcal{N}_{II} \in \mathcal{Q}^{\mathcal{E}_{V} * \mathcal{E}_{V} * \mathcal{T}_{V}}$ that locates the segmented regions in the given image.

$$\mathfrak{V}_{\mathcal{V}} = * \mathcal{N}_{\mathcal{V}-1} + bias_{\mathcal{V}} \tag{5}$$

The input images are processed using convolutional kernels with versions, and the input elements are released into the modern responsive location in accordance with equation (6). In this section the spatial values are $\hat{a} = \hat{o}$ – $[\mathbb{K}_{o-1}/2]$ and $\widehat{\mathbb{K}} = \widehat{\mathbb{K}} - [\mathbb{K}_{o-1}/2]$ are shown, taking into consideration o, \mathbb{W} , \hat{a} and $\widehat{\mathfrak{D}}$ which indicate the weights and coefficients over the given data or results.

$$\begin{split} \mathcal{Z}_{\chi}^{o,k,\mathfrak{w}} &= \sum_{\widehat{o},\widehat{\mathfrak{w}},\widehat{\mathfrak{w}}} \mathfrak{B}_{\chi}^{\widehat{o},\widehat{k},\widehat{\mathfrak{w}}} * \, \mathfrak{L}_{\chi-1}^{o+\widehat{o},k+\widehat{k},\widehat{\mathfrak{w}}} + bias_{\chi}^{\mathfrak{F}} \\ & \text{By modifying a few crucial patterns, the segmented} \end{split}$$

maps \mathcal{H}_{m} are finally obtained using the Ghosts module.

3.3. Feature Extraction Using Effective Net

The EfficientNet technique is a deep learning architecture that seeks to provide outstanding results on image classification problems while using minimal computer resources. It combines the principles of effective model design and compound scaling to balance model dimensions with performance. A basic convolutional neural network (CNN) architecture acts as the algorithm's starting point and is its basis. It is made up of convolutional, batch normalization, activation, and pooling layer-filled blocks that are continuously replicated. Efficient Net's merits can be shown in two different ways. It initially provides excellent precision. Furthermore, by lowering the dimensionality and floating-point computing cost, it improves the computational efficiency of the model. It is possible to create different versions of EfficientNet via compounding growth.

EfficientNet uses compound scaling, which increases the network's depth, width, and resolution simultaneously. A user-defined scaling parameter Ø and scaling coefficients α , β , γ , and, are used to adjust the scaling. Triple scaling is the use of a weighted scale with the three interconnected model hyperparameters, such as depth, width β , and resolution γ defined as follows, equation (7).

$$\alpha = A^{\emptyset}, \ \beta = B^{\emptyset}, \gamma = C^{\emptyset} \ r.s.t.\gamma^2 \approx 2$$

$$A \ge 1, B \ge 1, C \ge 1$$
(7)

Where the network's resolution is determined by the constants A, B, and C. Higher \emptyset values provide larger, more potent models, whilst lower values produce smaller, more effective models. The default compound configuration, EfficientNetB0, is defined when the compound coefficient \emptyset is set to 1. The co-efficient A, B, and C are optimized in the grid search in several ways:

$$A^*B^*C^* \approx 2 \tag{8}$$

And here is $A \ge 1$, $B \ge 1$, $C \ge 1$ under the conditions stated in (6), efficient net was able to attain the ideal values for A, B, and C as 1.2, 1.1, and 1.15, respectively. The scaled versions of EfficientNet can be achieved by changing the coefficient \emptyset in equation (8). The baseline EfficientNet architecture is utilized for feature extraction. The EfficientNet technique can be utilized for problems involving the accurate and effective detection of images of aortic aneurysm.

3.4. DBN Classifier

A Deep Belief Network (DBN) classifier is an instance of artificial neural network with several hidden unit layers. Usually, it consists of several layers of hidden units and one layer of visible units. Complex patterns and relationships in the input data are captured by DBNs, which are made to learn hierarchical representations of the data. It is constructed of one MLP layer and two RBM layers. Both the hidden and visible neurons in DBN lack connections with one another. MLP layer receives the output of RBM layer 2, while RBM layer 2 receives the output of the hidden layers of RBM layer 1. When the feature vector F is provided as input to the visible layer, the visible and hidden layers of RBM layer 1 are stated as follows: equation (9) and (10).

$$g^{1} = \{g_{1}^{1}, g_{2}^{1}, R, g_{n}^{1}, g_{f}^{1}\}, 1 \le n \le f;$$

$$(9)$$

$$h^{1} = \{h_{1}^{1}, h_{2}^{1}, R, h_{m}^{1}, R, h_{i}^{1}\}, 1 \le m \le j;$$

$$(10)$$

where f stands for the hidden neurons, g_n^1 for the n^{th} visible neuron at RBM layer 1, and h_m^1 for the m^{th} hidden neuron. Every neuron that is shown in both the visible and hidden layers has a bias.

The biases of the visible and hidden layers are represented by the variables x and y. For this reason, the two biases that represent the neurons at both layers are, equation (11) and (12).

$$g^{1} = \{g_{1}^{1}, g_{2}^{1}, R, g_{n}^{1}, g_{f}^{1}\}, 1 \le n \le f;$$

$$(11)$$

$$h^{1} = \{h_{1}^{1}, h_{2}^{1}, R, h_{m}^{1}, R, h_{i}^{1}\}, 1 \le m \le j;$$

$$(12)$$

where the bias corresponding to the m^{th} hidden neuron is indicated by h_m^1 , and the bias corresponding to the mth visible neuron is indicated by x_m^1 .

4. RESULT AND DISCUSSION

In this section, the assessment results of the aortic aneurysm detection are analysed and performance is discussed in terms of several evaluation criteria. The detection is found on a Windows operating system with an

Intel Core i7 CPU and 16 GB of RAM, using the Python programming language and libraries (Sci-Kit-Learn, TensorFlow, Keras, Numpy, HDF5, etc.). Using the dataset the effectiveness of the proposed system is evaluated.

4.1. Performance evaluation

Based on the qualities mentioned, a number of metrics are computed to assess performances.

The rate of correctly classifying a category is measured by accuracy. It is calculated by dividing the fraction of correctly classified categories across all classes by the total number of samples in the dataset.

$$Accuracy = \frac{TP + TN}{TP + TN + FP + FN} \tag{13}$$

The higher proportion of information is highlighted by precision. The formula (11) can be used to find the model Precision ratio.

$$Precision = \frac{TP}{TP + FP} \tag{14}$$

Recall is also known as Sensitivity or True Positive Rate (TPR), which is determined by applying equation, is related to the likelihood of finding intrusions.

$$Recall = \frac{TP}{TP + FN}$$
 Where, (15)

TP: Is a representation of the True Positive Predictive value.

TN: is a representation of a True Negative Predictive value.

FP: Is a representation of a False Positive Predictive value.

FN: is a representation of a False Negative Predictive value.

Table 1. Performance analysis of the proposed model

Classes	Accuracy	Precision	Recall
Normal	99.34%	98.63%	99.19%
Abnormal	99. 28%	98.57%	99.08%

The effectiveness evaluation of the proposed method is described in the Table 1 based on the accuracy, precision, and recall. The proposed archives an accuracy rate of 99.34% in the normal classes and 99.28% in the abnormal classes. Additionally, the proposed archives a precision and recall rate of 98.63% and 99.19% in normal classes and 98.57% and 99.08% in the abnormal classes.

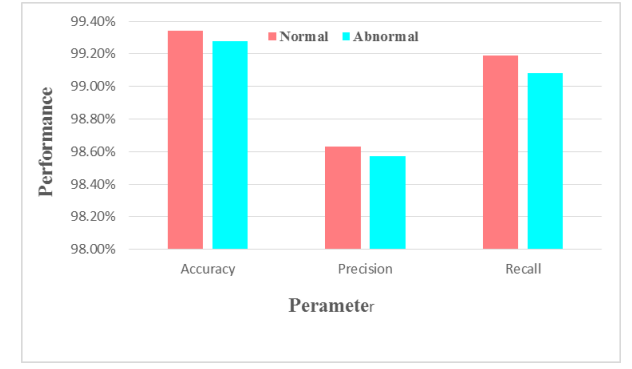


Figure 2. Performance evaluation of the proposed GOD-COCO model

Figure 2. describes the graphical representation of performance evaluation of the proposed using which results in high accuracy recall and precision in both normal and

abnormal classes. The proposed method archives an overall accuracy rate of 99.31% in the normal classes and abnormal classes.

4.2. Comparative Analysis

In this section, the existing methods was compared with the proposed model for the detection of AAA in its early stages based on the gathered dataset

Table 2. Comparison analysis of Existing methods vs Proposed method

Author	Methods	Accuracy
Brutti, F. et al	CTA	98.54%
Caradu, C. et al	PRAEVAorta	99.00%
Comelli, A et al	ATAAs	98.14%
Proposed method		99.31%

The comparison analysis between the suggested method and the current methods is shown in Table 2. The accuracy rating of 99.31% achieved by the suggested is higher than that of the current techniques. In this, the proposed achieves an overall accuracy rate of 0.77%, 0.31% and 1.17% over the existing methods such as CTA, PRAEVAorta and ATAAs respectively.

5. CONCLUSION

In this paper a novel has been proposed for detecting the abdominal aortic aneurysm. Initially the input CT images are pre-processed using AUG filter to enhance the quality of the images. Then the enhanced images are fed into Modified Deep V3+ for segmenting the required features from the image. The segmented images are inputted into feature extraction process for extracting the required features using Effective Net. Finally, the normal and abnormal classes of the aortic aneurysm detection is classified using DBN classifier. The proposed archives an accuracy rate of 99.34% in the normal classes and 99.28% in the abnormal classes. The accuracy rating of 99.31% achieved by the suggested is higher than that of the current techniques. In this, the proposed achieves an overall accuracy rate of 0.77%, 0.31% and 1.17% over the existing methods such as CTA, PRAEVAorta and ATAAs.

CONFLICTS OF INTEREST

The authors declare that there is no conflict of interest.

FUNDING STATEMENT

Authors did not receive any funding.

ACKNOWLEDGEMENTS

The author would like to express his heartfelt gratitude to the supervisor for his guidance and unwavering support during this research for his guidance and support.

REFERENCES

A. K. Golla, C. Tönnes, T. Russ, D. F. Bauer, M. F. Froelich,
 S. J. Diehl, S. O. Schoenberg, M. Keese, L. R. Schad, F. G.

- Zöllner, and J. S. Rink, "Automated screening for abdominal aortic aneurysm in CT scans under clinical conditions using deep learning", *Diagnostics*, vol. 11, no. 11, pp. 2131, 2021. [CrossRef] [Google Scholar] [Publisher Link]
- [2] I. M. Chiu, T. Y. Chen, Y. C. Zheng, X. H. Lin, F. J. Cheng, D. Ouyang, and C. Y. Cheng, "Prospective clinical evaluation of deep learning for ultrasonographic screening of abdominal aortic aneurysms", NPJ Digital Medicine, vol. 7, no. 1, pp. 282, 2024. [CrossRef] [Google Scholar] [Publisher Link]
- [3] T. Wang, W. Jin, F. Liang, and J. Alastruey, "Machine learning-based pulse wave analysis for early detection of abdominal aortic aneurysms using in silico pulse waves", *Symmetry*, vol. 13, no. 5, pp. 804, 2021. [CrossRef] [Google Scholar] [Publisher Link]
- [4] J. P. Pirruccello, M. D. Chaffin, E. L. Chou, S. J. Fleming, H. Lin, M. Nekoui, S. Khurshid, S. F. Friedman, A. G. Bick, A. Arduini, and L. C. Weng, "Deep learning enables genetic analysis of the human thoracic aorta", *Nature genetics*, vol. 54, no. 1, pp. 40-51, 2022. [CrossRef] [Google Scholar] [Publisher Link]
- [5] A. Abdolmanafi, A. Forneris, R. D. Moore, and E. S. Di Martino, "Deep-learning method for fully automatic segmentation of the abdominal aortic aneurysm from computed tomography imaging", Frontiers in Cardiovascular Medicine, vol. 9, pp. 1040053, 2023. [CrossRef] [Google Scholar] [Publisher Link]
- [6] M. Lindquist Liljeqvist, M. Bogdanovic, A. Siika, T. C. Gasser, R. Hultgren, and J. Roy, "Geometric and biomechanical modeling aided by machine learning improves the prediction of growth and rupture of small abdominal aortic aneurysms", *Scientific reports*, vol. 11, no. 1, pp. 18040, 2021. [CrossRef] [Google Scholar] [Publisher Link]
- [7] F. Lareyre, A. Chaudhuri, B. Nasr, and J. Raffort, "Machine learning and omics analysis in aortic aneurysm", *Angiology*, vol. 75, no. 10, pp. 921-927, 2024. [CrossRef] [Google Scholar] [Publisher Link]
- [8] T. Xiong, X. S. Lv, G. J. Wu, Y. X. Guo, C. Liu, F. X. Hou, J. K. Wang, Y. F. Fu, and F. Q. Liu, "Single-cell sequencing analysis and multiple machine learning methods identified G0S2 and HPSE as novel biomarkers for abdominal aortic aneurysm", Frontiers Immunology, vol. 13, pp. 907309, 2022. [CrossRef] [Google Scholar] [Publisher Link]
- [9] B. Li, R. Verma, D. Beaton, H. Tamim, M. A. J. J. Hussain, D. S. HoballahLee, D. N. Wijeysundera, C. de Mestral, M. Mamdani, and M. Al-Omran, "Predicting outcomes following endovascular abdominal aortic aneurysm repair using machine learning", *Annals Surgery*, vol. 279, no. 3, pp. 521-527, 2024. [CrossRef] [Google Scholar] [Publisher Link]
- [10] Z. Lyu, K. King, M. Rezaeitaleshmahalleh, D. Pienta, N. Mu, C. Zhao, W. Zhou, and J. Jiang, "Deep-learning-based image segmentation for image-based computational hemodynamic analysis of abdominal aortic aneurysms: a comparison study", *Biomedical Physics Eng. Express*, vol. 9, no. 6, pp. 067001, 2023. [CrossRef] [Google Scholar] [Publisher Link]
- [11] K. R. Akhila, N. Muthukumaran, & A. Ahilan, "Classification of Cervical Cancer Using an Autoencoder and Cascaded Multilayer Perceptron", *IETE J. Res.*, vol. 70, no. 1, pp. 26–36, 2023. [CrossRef] [Google Scholar] [Publisher Link]
- [12] N. Gopika Rani, N. Hema Priya, A. Ahilan & N. Muthukumaran, "LV-YOLO: logistic vehicle speed detection and counting using deep learning-based YOLO network",

Signal, Image Video Process., vol. 18, pp. 7419–7429, 2024. [CrossRef] [Google Scholar] [Publisher Link]

- [13] B. Joo, S. S. Ahn, P. H. Yoon, S. Bae, B. Sohn, Y. E. Lee, J. H. Bae, M. S. Park, H. S. Choi, and S. K., Lee, "A deep learning algorithm may automate intracranial aneurysm detection on MR angiography with high diagnostic performance", *European Radiology*, vol. 30, pp. 5785-5793, 2020. [CrossRef] [Google Scholar] [Publisher Link]
- [14] F. Brutti, A. Fantazzini, A. Finotello, L. O. Müller, F. Auricchio, B. Pane, G. Spinella, and M. Conti, "Deep learning to automatically segment and analyze abdominal aortic aneurysm from computed tomography angiography", *Cardiovascular Eng. Technol.*, pp. 1-13, 2022. [CrossRef] [Google Scholar] [Publisher Link]
- [15] C. Caradu, B. Spampinato, A. M. Vrancianu, X. Bérard, and E. Ducasse, "Fully automatic volume segmentation of infrarenal abdominal aortic aneurysm computed tomography images with deep learning approaches versus physician controlled manual segmentation", *J. Vascular Surgery*, vol. 74, no. 1, pp. 246-256, 2021. [CrossRef] [Google Scholar] [Publisher Link]
- [16] A. Comelli, N. Dahiya, A. Stefano, V. Benfante, G. Gentile, V. Agnese, G. M. Raffa, M. Pilato, A. Yezzi, G. Petrucci, and S. Pasta, "Deep learning approach for the segmentation of aneurysmal ascending aorta", *Biomedical Eng. Letters*, 11, pp. 15-24, 2021. [CrossRef] [Google Scholar] [Publisher Link]
- [17] P. G. Tahoces, R. Varela, and J. M. Carreira, "Deep learning method for aortic root detection", *Comput. Biology Medicine*, vol. 135, pp. 104533, 2021. [CrossRef] [Google Scholar] [Publisher Link]
- [18] S. Kim, Z. Jiang, B. A. Zambrano, Y. Jang, S. Baek, S. Yoo, and H. J. Chang, "Deep learning on multiphysical features and hemodynamic modeling for abdominal aortic aneurysm growth prediction", *IEEE Trans. Medical Imaging*, vol. 42, no. 1, pp. 196-208, 2022. [CrossRef] [Google Scholar] [Publisher Link]
- [19] T. Hu, M. Oda, Y. Hayashi, Z. Lu, K. K. Kumamaru, T. Akashi, S. Aoki, and K. Mori, Aorta-aware GAN for non-contrast to artery contrasted CT translation and its application to abdominal aortic aneurysm detection", *Int. J. Comput. Assisted Radiology Surgery*, pp.1-9, 2022. [CrossRef] [Google Scholar] [Publisher Link]

AUTHORS



J. Sworna Jo Lijha received her B.E Degree in Electronics and Communication Engineering and M.E Degree in Communication Systems from Anna University, Chennai, India in 2013 and 2015 respectively. Since 2015, she has started her career as an Assistant Professor, for the Department of Electronics and Communication Engineering in Arunachala College of Engineering for Women, Manavilai, Tamilnadu, India. From 2024, she has joined in Sree Sakthi Engineering College as Assistant

Professor for the Department of Electronics and Communication Engineering, at Coimbatore, Tamilnadu, India. She is currently doing her Ph.D. under the supervision of Dr.N.Muthukumaran. Her research interest includes deep learning, low light and medical image processing.



Muthukumaran was born Kaniyakumari, Tamilnadu, India, in 1984. He received the B.E Degree in Electronics and Communication Engineering, M.E Degree in Applied Electronics and the Ph.D Degree in Information and Communication Engineering from Anna University, Chennai, India in 2007, 2010 and 2015 respectively. He has 14 Years of Teaching and Research Experience and he is currently working as a Professor in the Department of Electronics Communication Engineering at Sri Eshwar

College of Engineering, Coimbatore, Tamilnadu, India. His major research interests are in the field of Digital Image/ Signal Processing, Multimedia Image/ Video Processing/ Compression, Digital and Analog Very Large-Scale Integration circuit design. Since 2006 he has published more than 73 International Journals like Springer, IEEE, Elsevier and 88 National/International conferences papers. He has published 15 International Books which is related to Engineering exclusively for Students and 27 Innovation Patents. He has actively participated and organized more than 102 research related events like National and International Workshop, Faculty Development Program, Seminar, Symposium, Conference and Short-Term Courses Delivered & Attended. He has collaborated and life time member for more than 19 various Memberships body Association like IEEE, ISI, WCECS, UACEE etc.

Arrived: 12.01.2025 Accepted: 15.02.2025